Polym. Bull. (2011) 66:239–258
DOI 10.1007/s00289-010-0351-5

ORIGINAL PAPER

# Effect of nano-nucleating agent addition on the isothermal and nonisothermal crystallization kinetics of isotactic polypropylene

**M. Ghorbanzadeh Ahangari · A. Fereidoon · N. Kordani · H. Garmabi**

Received: 4 February 2010 / Revised: 2 July 2010 / Accepted: 8 July 2010 /
Published online: 16 July 2010


**Abstract** Using differential scanning calorimetry (DSC) technique, a comparative study has been made of the isothermal and nonisothermal crystallization kinetics of nonnucleated isotactic polypropylene (iPP) and of nucleated iPP with 0.5 wt% of single-walled carbon nanotubes (SWCNTs) as a nucleating agent. The Avrami exponents ($n$) of iPP and nucleated iPP are close to 3.0 for isothermal crystallization. These results indicate that the addition of nucleating agents did not change the crystallization growth patterns of the neat polymer and that crystal growth was heterogeneous three-dimensional spherulitic. The results show that the addition of SWCNTs can shorten the crystallization half-time ($t_{1/2}$) and increase the crystallization rate of iPP. In the nonisothermal crystallization process, the Ozawa model failed to describe the crystallization behavior of nucleated iPP. The Cazé–Chuah model successfully described the nonisothermal crystallization process of iPP and its nanocomposite. A kinetic treatment based on the Ziabicki theory is presented to describe the kinetic crystallizability, in order to characterize the nonisothermal crystallization kinetics of iPP and nucleated iPP. Polarized light microscopy (PLM) experiments reveal that SWCNTs served as nucleating sites, resulting in a decrease of the spherulite size.

**Keywords** Isotactic polypropylene · Nanocomposite · Nucleating agent · Isothermal and nonisothermal crystallization kinetics · Crystal growth

M. Ghorbanzadeh Ahangari (✉) · A. Fereidoon · N. Kordani
Department of Mechanical Engineering, Semnan University, Semnan, Iran
e-mail: ghorbanzadeh.morteza@gmail.com

H. Garmabi
Department of Polymer Engineering, Amirkabir University of Technology, Tehran, Iran

## Introduction

The discovery of a new family of carbon structures, carbon nanotubes (CNTs), has broadened research in the field of material science [1–4]. Extensive research projects have been devoted to the use of CNTs as inorganic nanofillers to produce a variety of high-performance nanocomposites for targeted applications. Due to the high strength of the carbon–carbon bonds and their nearly perfect crystalline structure, these materials possess outstanding physical and mechanical properties [5, 6]. Previous theoretical studies of their mechanical properties have shown that their elastic modulus and tensile strength vary over quite broad ranges of 1–2 TPa and 37–200 GPa, respectively [7, 8]. The variations in the predicted mechanical properties of CNTs depend on the size and structure of the CNTs. There are two structures of CNTs: single-walled carbon nanotubes (SWCNTs) and multi-walled carbon nanotubes (MWCNTs). The nanotube walls of the former consist of only one layer of carbon atoms, while those of the latter are made of several concentric cylinders surrounding a hollow center [9].

Isotactic polypropylene (iPP), an important low-density, high-performance commercial semi-crystalline polymer, is widely used in food packaging, medical care, automobiles, and other industrial sectors [10–13].

Recently, polymer/CNTs nanocomposites have attracted considerable attention for their potential to achieve enhanced mechanical, thermal, and electrical properties as compared to those of conventional composites. Many parameters influence the effective properties of polymer/CNTs nanocomposites, e.g., CNTs structure, orientation, dispersion, diameter, adhesion of the CNTs to the matrix, and matrix stiffness [11–14].

Incorporated inorganic fillers, such as carbon black [15], talc [16], clay [17], and nano-$SiO_2$ [18], often act as nucleating agents for polymer crystallization. Many studies have been conducted using different methods to understand the influence of traditional nucleating agents on the kinetics of polymer crystallization [19, 20]. Li et al. [21] studied the isothermal crystallization kinetics of iPP nucleated with carbon black. Yuan et al. [22] studied the effect of clay on the nonisothermal crystallization kinetics of polypropylene. Knowledge of the effects of such nucleating agents on isothermal and nonisothermal crystallization is useful for determining processing conditions and for evaluating the effectiveness of the nucleating agents. However, during the processing of polymer materials, the crystallization processes generally proceed under nonisothermal conditions; thus, studies of the nonisothermal kinetics are often useful complements for understanding the crystallization behavior of a polymer during its processing.

We prepared pure iPP and a SWCNTs-filled nanocomposite based on iPP by a melt-mixing method. In this study, we aimed to investigate the isothermal and nonisothermal crystallization kinetics of iPP and the nanocomposite containing SWCNTs, as studied by differential scanning calorimetry (DSC). The crystallization kinetic parameters and thermal characteristics based on the isothermal crystallization of iPP and the nanocomposite were studied according to the Avrami model. In addition, the experimental data were analyzed based on the Ozawa, Cazé–Chuah, and Ziabicki models for nonisothermal crystallization. The spherulitic morphology

of samples under isothermal crystallization conditions were also examined using polarized light microscopy (PLM).

## Experimental

### Materials

The iPP homopolymer was supplied by Bandar Imam Petrochemical Co., Iran, as grade Poliran PI0800, with a melt flow index and density of 8 g/10 min and 0.902 g/cm$^3$, respectively. The raw materials were obtained from commercial sources. The SWCNTs were provided by the Research Institute of the Petroleum Industry (RIPI), Iran. The SWCNTs were prepared using a chemical vapor deposition (CVD) process, with a methane carbon source, a cobalt and molybdenum catalyst system, and a reaction temperature between 800 and 1000 °C. The SWCNTs produced were washed with HCl and distilled water to yield >90% purity. The resulting SWCNTs diameters were between 1 and 4 nm and the maximum length was less than 10 μm.

### Blend preparation

Prior to the preparation of the nanocomposites, iPP and SWCNTs were dried in a vacuum oven for 12 h at 80 °C. The mixing of the components was performed in an internal mixer (Haake Rheomix; HBI SYS90) with a rotor speed of 120 rpm at 180 °C. The iPP granules and SWCNTs (0.5 wt%) were all dry-blended first and then introduced into the mixer and mixed for 10 min. The mixture was compression-molded after the mixing was complete. A square plaque of the mixture was prepared in a Toyoseiki Mini Test Hydraulic Press at 190 °C and 10 MPa for 5 min. The sheets were then directly quenched at room temperature.

### Methods

Thermal analysis was carried out using a Perkin-Elmer DSC (model Pyris I) interfaced with a personal computer. The temperature scale of the calorimeter was calibrated with indium. All of the samples were weighed (5 ± 0.2 mg) and enclosed in an aluminum pan. An empty aluminum pan was also used as a reference. The isothermal samples were heated to 210 °C and, to ensure complete melting, kept at this temperature for 5 min to eliminate the effect of the heat history. After this period, samples were rapidly cooled at the crystallization temperature and maintained at that for the time necessary for complete crystallization of the samples. The nonisothermal samples were first heated to 210 °C, held at this temperature for 5 min and then cooled at a rate of 2.5–50 °C min$^{-1}$ to determine the crystallization temperature ($T_p$). The exotherms were recorded as a function of temperature for further analysis according to isothermal and nonisothermal models.

For the observation of spherulitic morphology, a Carl Zeiss Jena (Jenapol) PLM system equipped with a Linkam THMS 600 hot stage and a TMS 92 temperature

controller was used. Thin films (approximately 10 μm thick) of each sample were sandwiched and melted between microscope glass covers at 210 °C for 5 min and then rapidly cooled to the desired isothermal crystallization temperature.

## Results and discussion

### Isothermal crystallization behavior

The isothermal melt crystallization exotherms for iPP and nucleated iPP with 0.5 wt% of SWCNTs at different temperatures are shown in Fig. 1. The effect of temperature on the crystallization rate of iPP is clearly shown in the isothermal thermograms. With an increase in the crystallization temperature, the exothermal peak of the DSC curves shifts obviously to the right, which indicates that the crystallization time was increased and the crystallization rate was decreased. Generally, this behavior can be attributed to the decrease of nucleation density and growth rate of the spherulites at higher temperature. The relative crystallinity at time $t$ ($X_t$) was obtained from the area under the exotherm up to time $t$, divided by the total area under the exotherm [23]:

$$X_t = \frac{\int_0^t \frac{dH_c}{dt} \cdot dt}{\int_0^\infty \frac{dH_c}{dt} \cdot dt} \tag{1}$$

where $\frac{dH_c}{dt}$ is the heat evolution rate. The development of the relative crystallinity at time $t$ for iPP and nucleated iPP is shown in Fig. 2. The effect of temperature on the crystallization rate is even more evident in the relative crystallinity curves in Fig. 2.

The isothermal crystallization from the melt for various modes of nucleation and growth can be well approximated by the Avrami equation [24–26]:

$$1 - X_t = \exp[-Zt^n] \tag{2}$$

where $n$, the Avrami exponent, is a constant that depends on the mechanism of nucleation and the form of crystal growth and $Z$ is the Avrami rate constant.

Taking the logarithm of Eq. 2 gives

$$\log[-\ln(1 - X_t)] = n \log t + \log Z \tag{3}$$

The crystallization half-life time $t_{1/2}$ is defined as the time required to reach half of the final crystallinity and was determined from Fig. 2 and the measured kinetics parameters. That is,

$$t_{1/2} = \left(\frac{\ln 2}{Z}\right)^{1/n} \tag{4}$$

Using the plot of $\log[-\ln(1 - X_t)]$ versus $\log t$, the Avrami parameters $n$ and $Z$ were determined from the slope and intercept of these straight lines (Fig. 3). The values of $n$, $Z$, and $t_{1/2}$ are listed in Table 1. For iPP and nucleated iPP, the average values of the Avrami parameter $n$ were equal to 2.52 and 3.18, respectively. These values of $n$ ($n = 3$) are characteristic of a crystallization process with

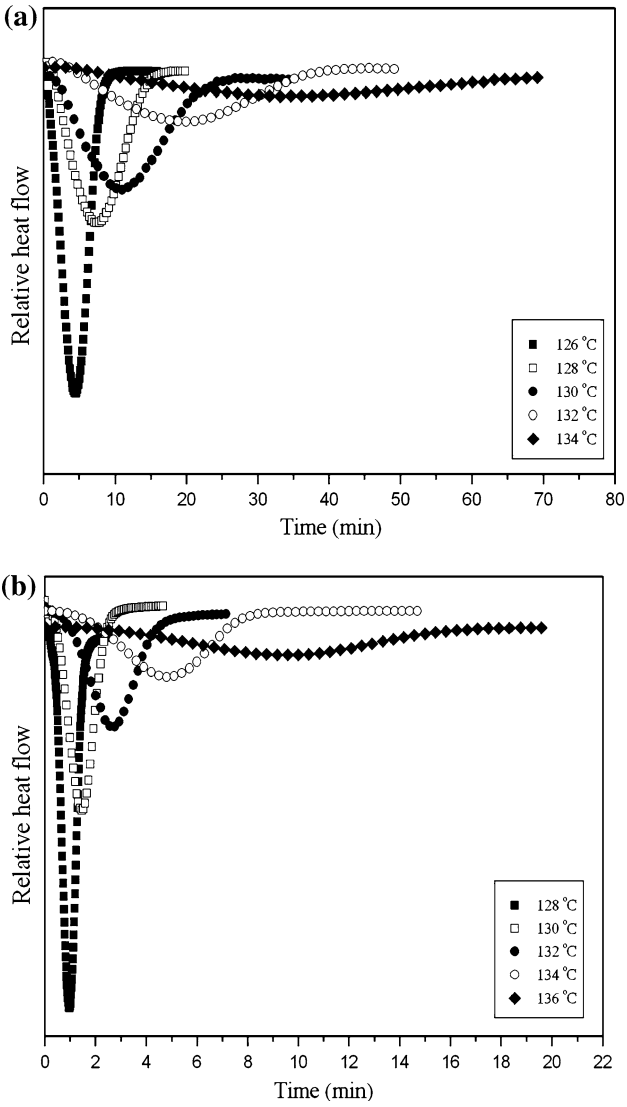


**Fig. 1** DSC scans during isothermal crystallization at different crystallization temperatures for **a** iPP and **b** iPP/SWCNTs nanocomposite

three-dimensional spherical growth with heterogeneous nucleation [27]. No significant changes in the values of $n$ were found with the addition of SWCNTs; thus, the addition of SWCNTs may not affect the geometric dimension of iPP crystal growth. The values of $Z$ increased and the $t_{1/2}$ value decreased upon adding SWCNTs to the iPP matrix. These results are consistent with the fact that the crystallization rate of nucleated iPP is higher than that of the pure iPP. This can be attributed to the nucleation effect of SWCNTs on the crystallization of iPP.

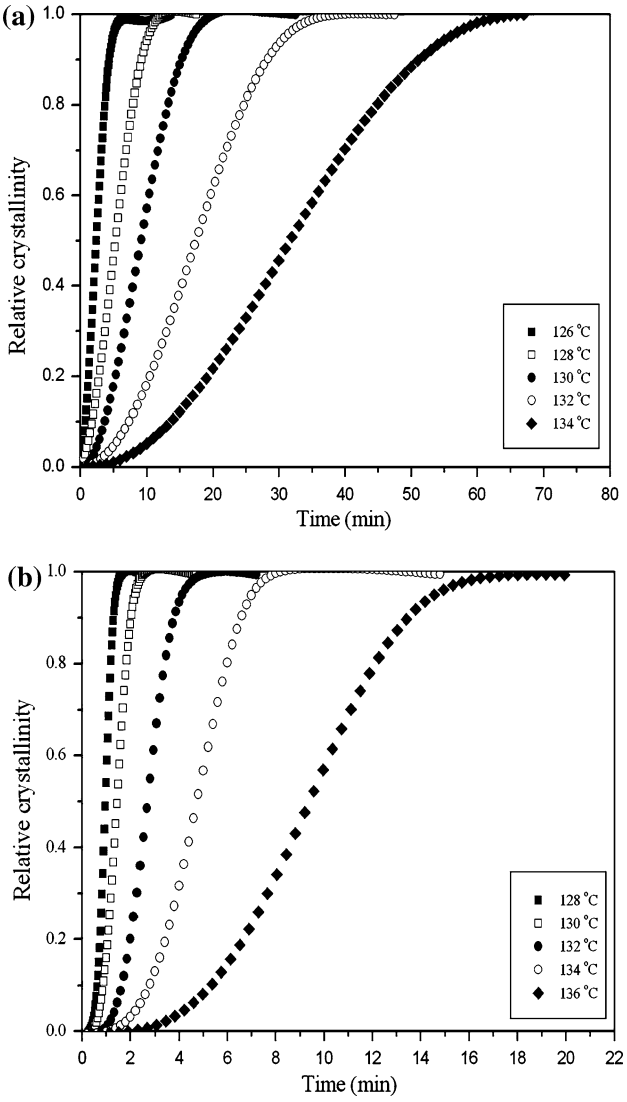


**Fig. 2** Development of Relative crystallinity versus time for **a** iPP. **b** iPP/SWCNTs nanocomposite during isothermal crystallization

Additionally, the data show that, with increasing crystallization temperature, the $Z$ values of all samples decreased and those of $t_{1/2}$ increased. This is consistent with the fact that iPP crystallizes more slowly when the crystallization temperature is increased.

Polarized light microscopy (PLM) is one of the predominant and most informative methods for investigating spherulitic morphologies. PLM images of the crystals produced by the crystallization of iPP and the nucleated polymer at 132

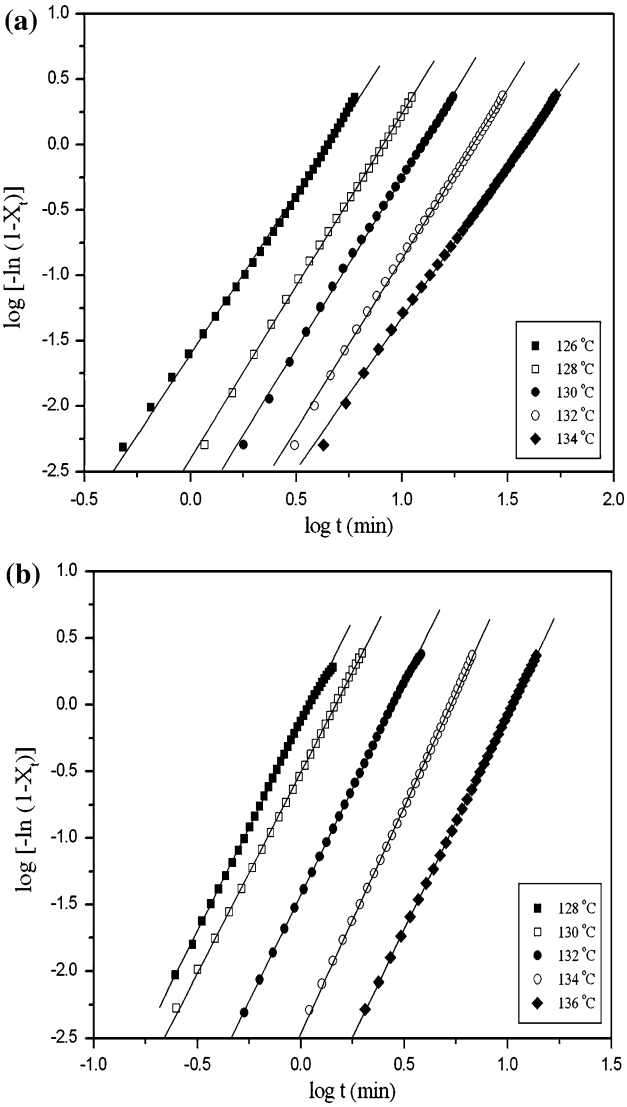


**Fig. 3** Plots of $\log[-\ln(1 - X_t)]$ versus $\log t$ for isothermal crystallization of **a** iPP. **b** iPP/SWCNTs nanocomposite

and 136 °C are shown in Fig. 4a, b, respectively. As shown in Fig. 4a, the iPP polymer formed spherulites when it was crystallized from the melt. Figure 4b also shows that, for the nanocomposite, many spherical-shaped crystals were formed in the temperature range studied. It can be established that the iPP/SWCNTs nanocomposite had the same spherulitic structure as the pure iPP, but the nanocomposite differed in that it had much smaller and more numerous spherulites.

**Table 1** Isothermal kinetic parameters of iPP and iPP/SWCNTs nanocomposite

| Sample | $T_p$ (°C) | Log $Z$ | $n$ | $t_{1/2}$[a] (min) | $t_{1/2}$[b] (min) |
|---|---|---|---|---|---|
| iPP | 126 | −1.60 | 2.46 | 3.92 | 3.85 |
| | 128 | −2.40 | 2.63 | 7.13 | 7.11 |
| | 130 | −2.87 | 2.62 | 10.87 | 10.83 |
| | 132 | −3.48 | 2.59 | 19.06 | 19.15 |
| | 134 | −3.65 | 2.32 | 32.13 | 31.97 |
| Average | | | 2.52 | | |
| iPP/SWCNTs | 128 | −0.14 | 3.10 | 1.01 | 0.99 |
| | 130 | −0.51 | 3.08 | 1.31 | 1.30 |
| | 132 | −1.43 | 3.18 | 2.47 | 2.51 |
| | 134 | −2.44 | 3.33 | 4.80 | 4.84 |
| | 136 | −3.30 | 3.22 | 9.45 | 9.45 |
| Average | | | 3.18 | | |

[a] Obtained from crystallization exotherms

[b] Calculated from Eq. 4

The much smaller size of the spherulites proves that the SWCNTs act as a nucleating agent in the polymer matrix. These results obtained from PLM are in accordance with our earlier analysis.

## Nonisothermal crystallization behavior

The nonisothermal melt crystallization exotherms for iPP and the iPP/SWCNTs nanocomposite with a 0.5 wt% content of SWCNTs at different cooling rates are shown in Fig. 5. As the cooling rate increased, the exothermic traces became wider and shifted towards lower temperatures for both iPP and the nanocomposite studied. In all cases, the peak crystallization temperature, $T_p$, which corresponds to the maximum crystallization rate, decreased with an increase in cooling rate, indicating that the crystallization process is controlled by the nucleation rate. For example, $T_p$ of neat iPP decreased by about 15.5 °C when the cooling rate increased from 2.5 to 40 °C min$^{-1}$. The high $T_p$ values at low cooling rates indicate that crystallization was initiated at an early stage. The lower cooling rate provides sufficient time for the polymer chains to align themselves. Figure 5 shows that $T_p$ increased with the addition of SWCNTs into the pristine polymer. For example, at a cooling rate of 10 °C min$^{-1}$, the crystallization peak temperature for pure iPP was 115.9 °C, while for the iPP/SWCNTs nanocomposite, it was 124.6 °C. The values of $T_p$ and the crystallization enthalpy $\Delta H_c$ are listed in Table 2. This behavior may be attributed to the surface of the SWCNTs, which easily adsorbs the iPP chain segments and acts as an effective nucleating agent, thus allowing the crystallization of iPP molecules to occur at a higher crystallization temperature, as shown in Fig. 5 [28, 29].

Several methods, such as the modified Avrami equation [30], the Ozawa method [31], the Cazé–Chuah method [32, 33], and others [34, 35], have been proposed in order to analyze the nonisothermal crystallization kinetics of different materials.

We have discussed the isothermal crystallization kinetics for iPP and its nanocomposite. This section discusses the nonisothermal crystallization kinetics.

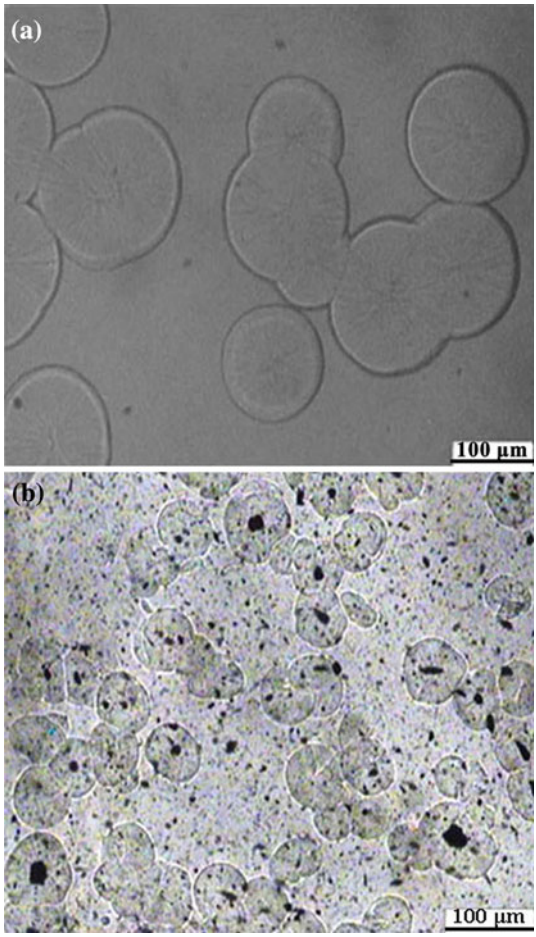


**Fig. 4** PLM micrograph after isothermal crystallization of **a** iPP at 132 °C. **b** iPP/SWCNTs nanocomposite at 136 °C

Figure 6 shows the relative degree of crystallinity as a function of temperature for iPP and the iPP/SWCNTs nanocomposite at various cooling rates.

By assuming that the nonisothermal crystallization process can be comprised of infinitesimally small isothermal crystallization steps, Ozawa modified the Avrami equation by taking into account the effect of the cooling rate on the crystallization process from the molten to the glassy state [31]

$$1 - X_t = \exp\left(\frac{-K(T)}{\Phi^m}\right) \tag{5}$$

where $m$ is the Ozawa exponent, which depends on the dimension of the crystal growth and the nucleation mechanism, and $K(T)$ is a function of the cooling rate. By taking the double logarithmic form, we obtain the following relationship:

$$\log[-\ln(1 - X_t)] = \log\ K(T) - m \log \Phi \tag{6}$$

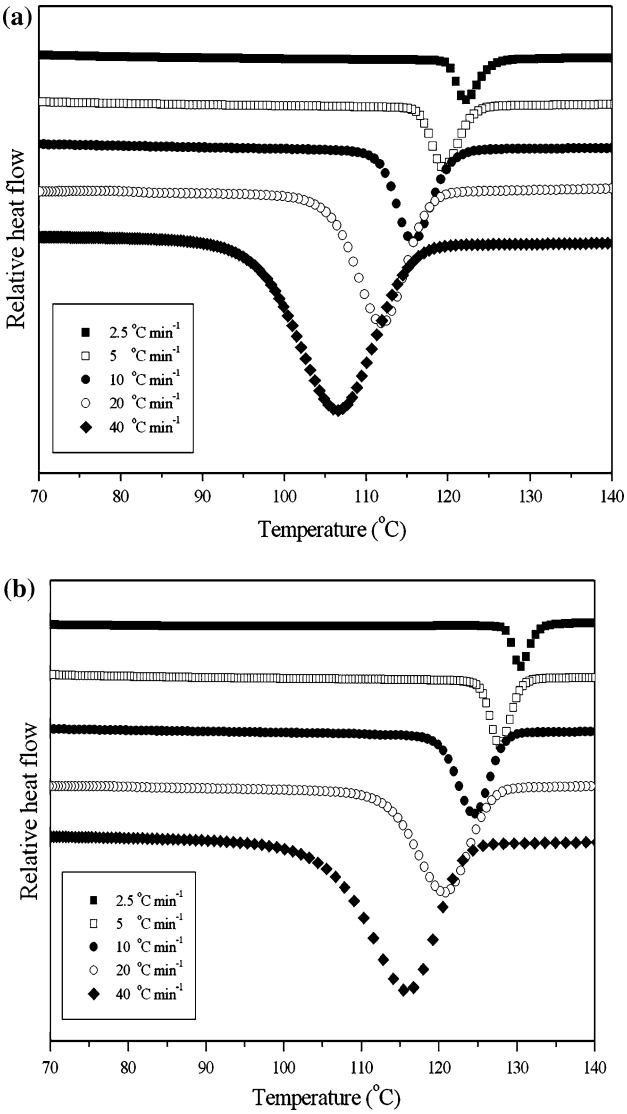


**Fig. 5** DSC scans during nonisothermal crystallization at different cooling rates for **a** iPP. **b** iPP/SWCNTs nanocomposite

Plotting $\log[-\ln(1 - X_t)]$ versus $\log \Phi$ at a given temperature should yield a straight line if the Ozawa method is valid, with $K(T)$ and $m$ as the intercept and slope, respectively. By plotting $\log[-\ln(1 - X_t)]$ versus $\log\Phi$ (Fig. 7a), a series of straight lines was obtained. Thus, pristine iPP nonisothermal crystallization could be fitted with the Ozawa method. In addition, the results based on the Ozawa analysis for the nanocomposite showed some obvious deviations (Fig. 7b). The nonlinear plots suggest that $m$ was not constant with temperature during the primary crystallization

**Table 2** Non-isothermal kinetic parameters of iPP and iPP/SWCNTs nanocomposite based on Ziabicki analysis

| Sample | Φ (°C/min) | $T_p$ (°C) | $\Delta H$ (J/g) | $T_{\Phi,max}$ (°C) | $(dX/dT)_{\Phi,max}$ ($S^{-1}$) | $D_\Phi$ (°C) | $G_{Z,\Phi}$ | $G_Z$ |
|---|---|---|---|---|---|---|---|---|
| iPP | 2.5 | 122.2 | 112.7 | 122.2 | 0.3 | 2.9 | 0.926 | 0.370 |
| | 5 | 119.7 | 103.7 | 119.7 | 0.25 | 3.6 | 0.958 | 0.192 |
| | 10 | 115.9 | 101.1 | 115.6 | 0.18 | 5.1 | 0.977 | 0.098 |
| | 20 | 112.9 | 98.4 | 112.2 | 0.13 | 6.9 | 0.954 | 0.048 |
| | 40 | 106.7 | 90.8 | 107.7 | 0.09 | 10.5 | 1.005 | 0.025 |
| Average | | | | | | | | 0.147 |
| iPP/SWCNTs | 2.5 | 130.5 | 110.8 | 130.5 | 0.37 | 2.4 | 0.945 | 0.378 |
| | 5 | 127.9 | 101.6 | 128.0 | 0.30 | 3.0 | 0.958 | 0.192 |
| | 10 | 124.6 | 97.3 | 124.7 | 0.19 | 4.7 | 0.950 | 0.095 |
| | 20 | 121.0 | 99.7 | 120.9 | 0.12 | 7.6 | 0.970 | 0.049 |
| | 40 | 116.2 | 97.5 | 116.8 | 0.09 | 9.9 | 0.948 | 0.024 |
| Average | | | | | | | | 0.148 |

process. Thus, the secondary crystallization of the iPP/SWCNTs nanocomposite should not be neglected. The slope varies with temperature during crystallization; that is, the Ozawa method still cannot satisfactorily express the nonisothermal crystallization process of the iPP/SWCNTs nanocomposite.

Cazé et al. [32] proposed a novel approach to treat the nonisothermal crystallization. According to Cazé, the nonisothermal crystallization can be described by

$$1 - X_v = \exp\left[\frac{-K(T)}{\Phi^m}\right] \tag{7}$$

where $X_v$ is the volume-fractional crystallinity. By assuming that $K(T)$ exponentially increases with crystallization temperature, $T$, upon cooling, and that the exotherm curve has a slanted Gaussian shape, the peak crystallization temperature is linearly related to ln Φ with a slope of $m$. However, this treatment seems to be useful only for $\Phi < 10$ °C $min^{-1}$ for both unfilled and filled iPP due to the superposition of crystallization regimes I and II at higher Φ.

Based on the relative crystallinity at time $t$, which was obtained via the previously described method, the volume fraction $X_v$ can be derived by [36]

$$X_v = X_t(\rho_a/\rho_c)[1 - (1 - \rho_a/\rho_c)X_t]^{-1} \tag{8}$$

where $\rho_a$ and $\rho_c$ are the bulk densities of the polymer in the pure amorphous and crystalline states, respectively. By considering the influence of the crystallization temperature, $\rho_a/\rho_c$ was modified as [33]:

$$\rho_a/\rho_c = (\rho_{a0}/\rho_{c0}) \exp\left[(T - T_r)\left(0.11/T_m^0 - 0.16/T_g\right)\right] \tag{9}$$

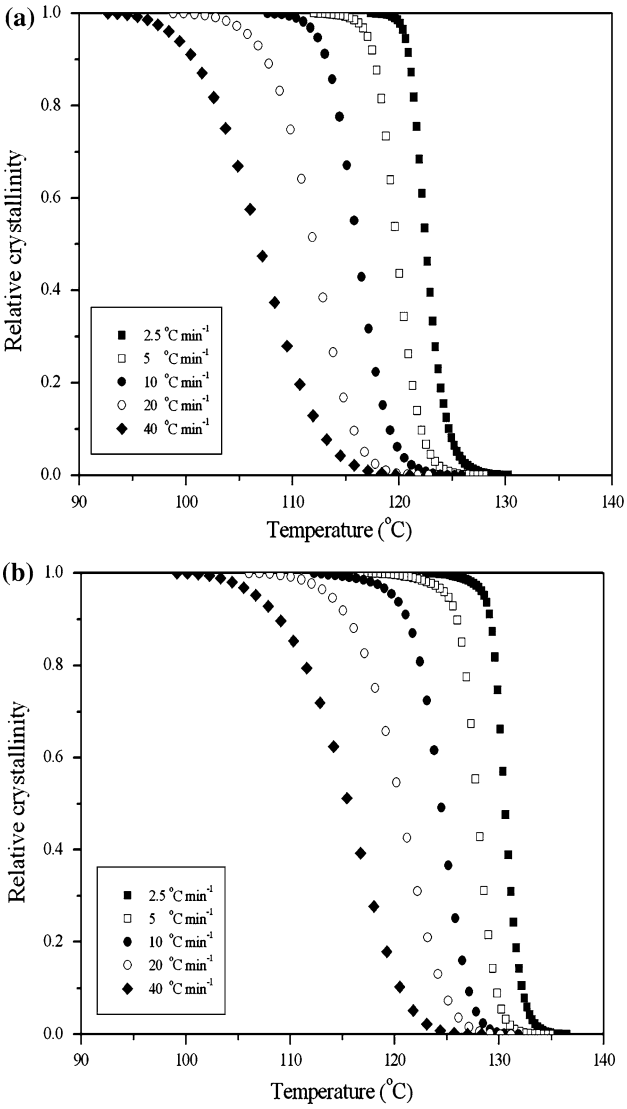


**Fig. 6** Development of relative crystallinity versus temperature for **a** iPP. **b** iPP/SWCNTs nanocomposite during nonisothermal crystallization

where $\rho_{a0}$ and $\rho_{c0}$ refer to the densities of $\rho_a$ and $\rho_c$, respectively, at the reference temperature $T_r$. For iPP, when $T_r$ is equal to 298 K, $\rho_{a0} = 0.850$ g cm$^{-3}$, $\rho_{c0} = 0.936$ g cm$^{-3}$ $T_m^0 = 444.2$ K, and $T_g = 256.2$ K [36].

Chuah et al. [33] modified this method and applied it to successfully describe the nonisothermal crystallization of different kinds of polymers as follows:

$$\ln K(T) = \beta(T - T_1) \tag{10}$$

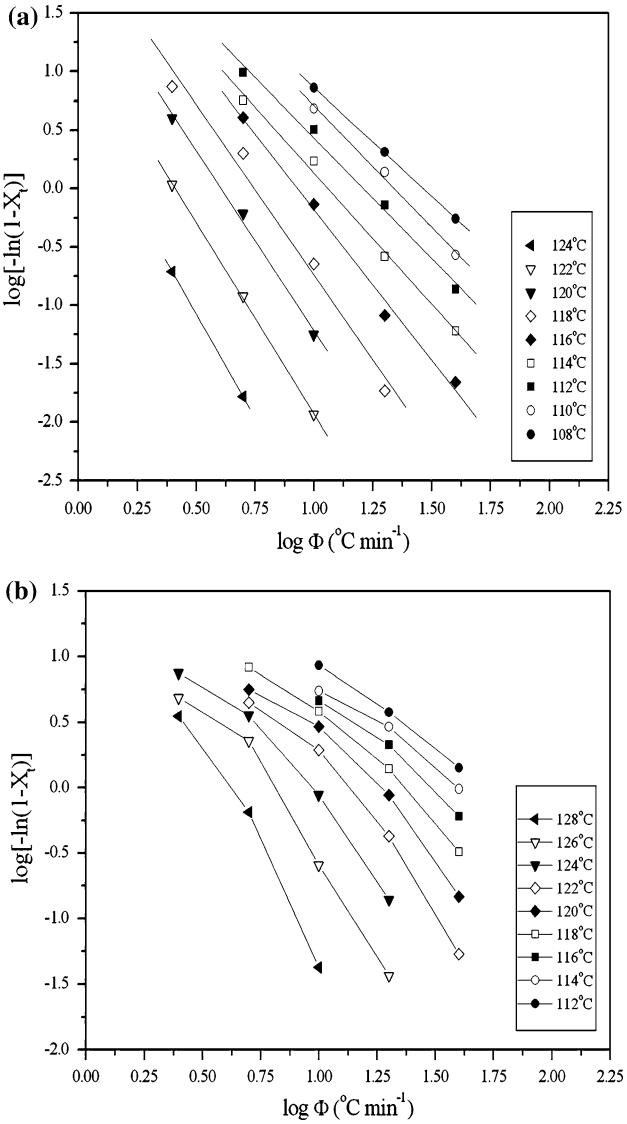


**Fig. 7** Analysis of the Ozawa model for **a** iPP. **b** iPP/SWCNTs nanocomposite at the indicated temperatures

where $\beta$ and $T_1$ are the experimental constants. Letting $\left(\frac{\partial^2 X_v}{\partial^2 T^2}\right)_{T_p} = 0$, the $K(T)$ can be

$$K(T)|_{T_p} = \Phi^m \tag{11}$$

Thus, by combining Eqs. 7, 10, and 11

$$\ln[-\ln(1 - X_v)] = \beta(T - T_p) \tag{12}$$

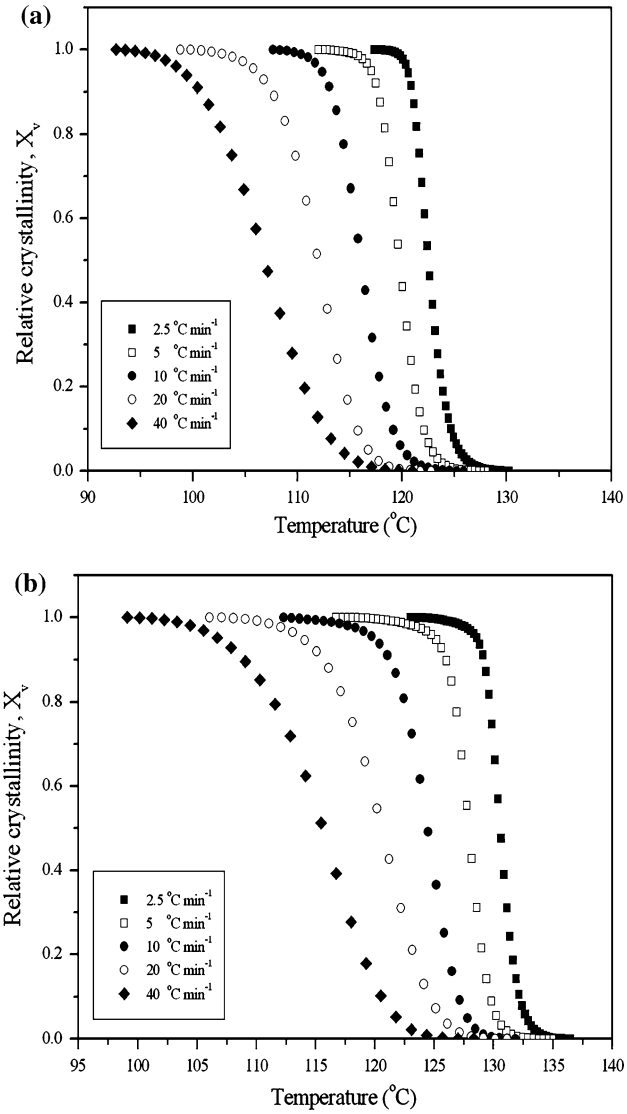


**Fig. 8** Development of volume fractional crystallinity as a function of temperature for nonisothermal crystallization for **a** iPP. **b** iPP/SWCNTs nanocomposite

Then, drawing the straight line corresponding to $\ln[-\ln(1 - X_v)]$ versus $T$ by using Eq. 12, we can derive the values of $\beta$ and $-\beta T_p$ from the slope and intersect. Another equation obtained by combining Eqs. 11 and 12 can be written as follows:

$$T_p = m \ln \Phi/\beta + T_1 \tag{13}$$

where $T_1$ is $T_p$ at $\Phi = 1$ °C min$^{-1}$. Plotting $T_p$ versus $\ln \Phi/\beta$ should yield a straight line with slope $m$. Figure 8 shows the plot of $X_v$ versus $T$ for the crystallization of virgin and nucleated iPP at different cooling rates. The plots of $\ln[-\ln(1 - X_v)]$

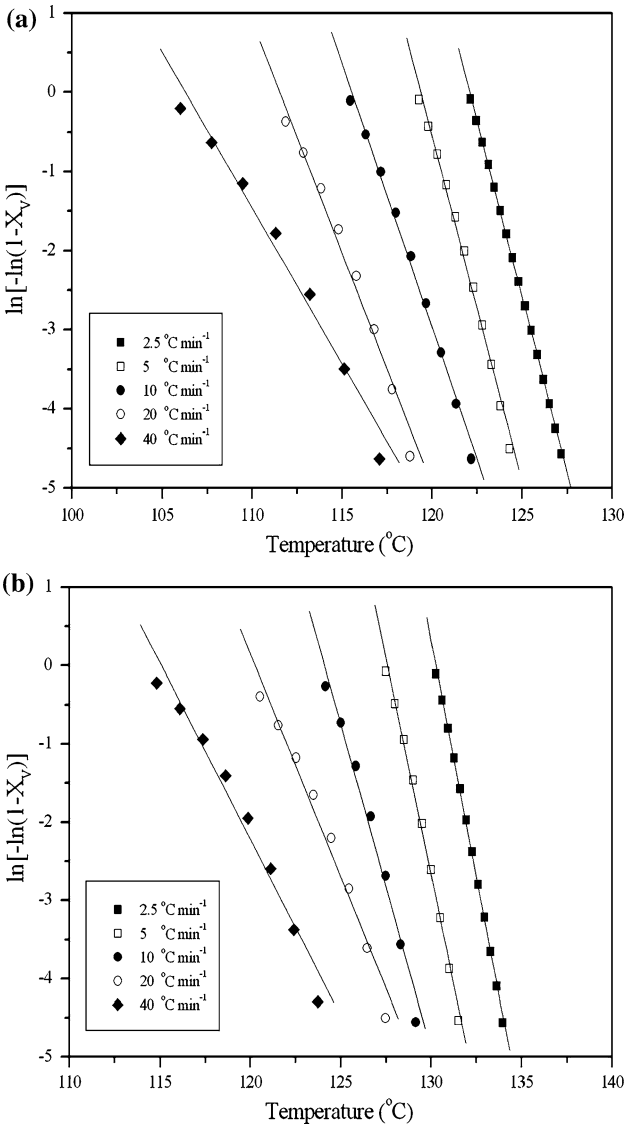


**Fig. 9** Plots of $\ln[-\ln(1 - X_v)]$ versus temperature for **a** iPP. **b** iPP/SWCNTs nanocomposite

versus $T$ for these two materials are shown in Fig. 9, from which a series of $T_p$ and $\alpha$ can be derived. Figure 10 illustrates the form of $T_p$ versus $\ln \Phi/\beta$. The calculated average values of $m$ obtained from the Cazé–Chuah method were approximately 2.61 and 2.70 for iPP and the iPP/SWCNTs nanocomposite, respectively. These values are close to the integer 3 and are consistent with three-dimensional crystal growth from heterogeneous nuclei as well as with the Avrami analysis results

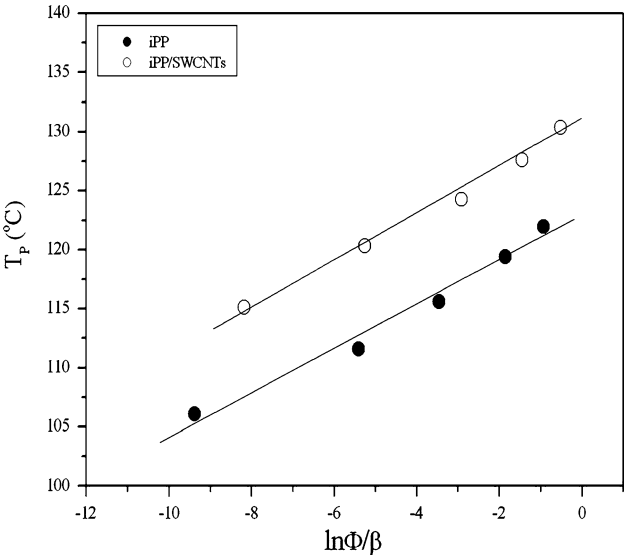


**Fig. 10** Plots of peak crystallization temperature versus ln $\Phi/\beta$

obtained under isothermal crystallization kinetic conditions. This uniformity of crystalline dimension could be attributed to the stability of the nucleation process because of much lower SWCNTs concentration.

Ziabicki [37, 38] suggested that the nonisothermal crystallization process of polymer phase transportation can be represented by a first-order kinetic equation such as:

$$\frac{dX_t}{dt} = P(T)[1 - X_t] \tag{14}$$

where $P(T)$ is a temperature-dependent crystallization rate function. For nonisothermal crystallization, the two parameters vary with the cooling rate used.

Ziabicki showed that, for a given cooling condition, it is possible to describe $P(T)$ with a Gaussian function of the form

$$P(T) = P_{\max} \exp\left[-4 \ln 2 \frac{(T - T_{\max})^2}{D^2}\right] \tag{15}$$

where $T_{\max}$ is the temperature at which the maximum rate of crystallization occurs, $P_{\max}$ is the crystallization rate at $T_{\max}$, and $D$ is the half-width of the crystallization rate–temperature function. Integration of the above equation for a given cooling condition over the entire range of crystallization temperatures ($T_g \prec T \prec T_m^0$) results in an important characteristic value for the crystallization ability, $G_Z$, of semi-crystalline polymers, which can be expressed in the following form:

$$G_Z = \int_{T_g}^{T_m^0} P(T)\ \mathrm{d}T \approx 1.064 P_{\max} D \tag{16}$$

Based on the approximation theory, the degree of crystallinity, determined when the polymer is cooled from melting to the glass transition temperature at a unit cooling rate, is characterized by the kinetic crystallizability, $G_Z$.

The above equation can be applied to nonisothermal crystallization when $P_{\max}$ is substituted with a derivative function of $(\mathrm{d}X_t/\mathrm{d}T)_\Phi$ specific for each cooling rate studied.

Therefore, the above equation can be rewritten as

$$G_{Z,\Phi} = \int_{T_g}^{T_m^0} (\mathrm{d}X_t/\mathrm{d}T)_\Phi \mathrm{d}T \approx 1.064 (\mathrm{d}X_t/\mathrm{d}T)_{\Phi,\max} D_\Phi \tag{17}$$

where $(\mathrm{d}X_t/\mathrm{d}T)_{\Phi,\max}$ and $D_\Phi$ are the maximum crystallization rate and the half-width of the derivative of relative crystallinity as a function of temperature, $(\mathrm{d}X_t/\mathrm{d}T)_\Phi$, respectively, $T_g$ is the glass transition temperature, and $T_m^0$ is the equilibrium melting temperature. Figure 6 can be converted into Fig. 11, which shows the crystallization rate $(\mathrm{d}X_t/\mathrm{d}T)_\Phi$ as a function of temperature $T$ by differentiating each profile in Fig. 6. From Fig. 11, $(\mathrm{d}X_t/\mathrm{d}T)_{\Phi,\max}$ and $D_\Phi$ can be obtained, and then $G_{Z,\Phi}$ can be calculated using Eq. 17. Thus, the kinetic crystallizability, $G_Z$, at a unit cooling rate can also be obtained by normalizing $G_{Z,\Phi}$ with $\Phi$, as listed in Table 2. Based on the average of the values of $G_Z$ summarized in Table 2, the crystallization abilities for both studied samples were approximately the same. These results show that the value of $G_Z$ is not strongly influenced much by the presence of SWCNTs in the polymer matrix.

## Conclusion

The isothermal and nonisothermal crystallization behaviors of neat iPP and melt-blended iPP/SWCNTs nanocomposites containing 0.5 wt% SWCNTs were studied by DSC. The results obtained from an Avrami analysis under isothermal crystallization conditions indicate that the addition of a nucleating agent into the polymer matrix can increase the crystallization rate and decrease the crystallization half-time of iPP remarkably. The Avrami exponent $n = 3$ was obtained for the isothermal crystallization process for the samples, and the process of crystal growth was three-dimensional heterogeneous in both non-nucleated and nucleated iPP. From PLM observations, it can be established that the nucleated iPP has the same spherulitic morphology as the pure iPP, but the nucleated iPP differed in that it had much smaller and more numerous spherulites.

The nonisothermal crystallization processes of the polymer and its nanocomposite were successfully determined by means of the Cazé–Chuah and Ziabicki models. The Ozawa model does not fit for the nonisothermal crystallization process

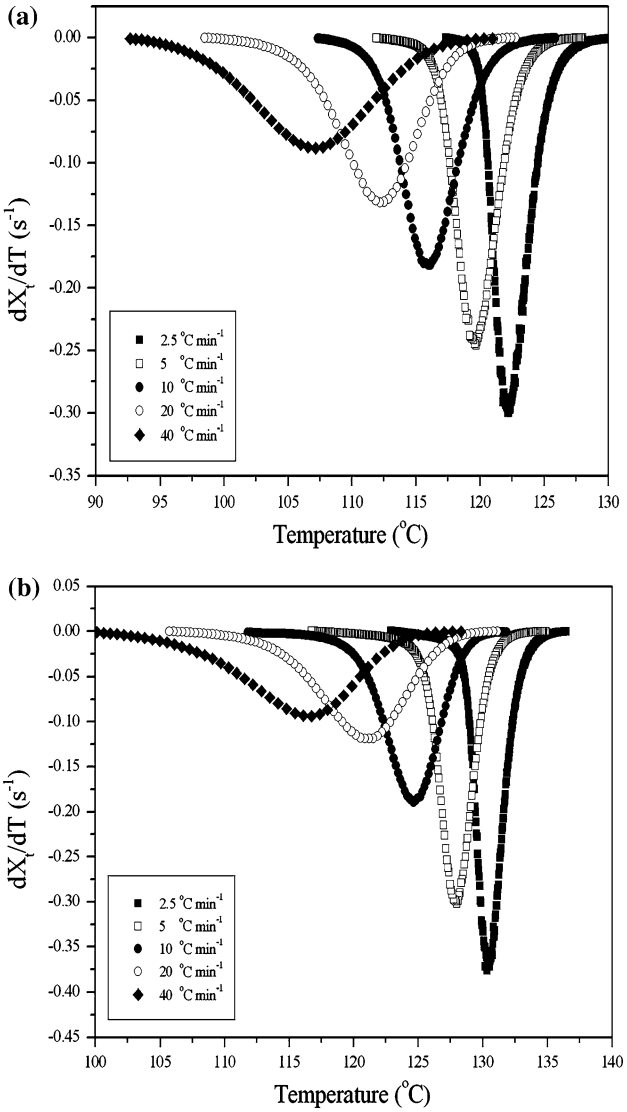


**Fig. 11** Crystallization rate as a function of temperature for **a** iPP. **b** iPP/SWCNTs nanocomposite at different cooling rates

of the nanocomposite. The Cazé–Chuah analysis results showed that the value of the Ozawa exponent, *m*, was equal to 3 for the nonisothermal crystallization process for iPP and the iPP/SWCNTs nanocomposite, indicating that the mode of spherulitic growth mechanisms does not change than that of isothermal crystallization process for the samples. The results from the Ziabicki analysis showed that the crystallization abilities of iPP and the iPP/SWCNTs nanocomposite are equivalent to each other.

## References


1. Bao SP, Tjong SC (2008) Mechanical behavior of polypropylene/carbon nanotube nanocomposites: the effect of loading rate and temperature. Mater Sci Eng A 485:508–516
2. Li L, Li CY, Ni C, Rong L, Hsiao B (2007) Structure and crystallization behavior of Nylon 66/multi-walled carbon nanotube nanocomposites at low carbon nanotube contents. Polymer 48:3452–3460
3. Leelapornpisit W, Ton-That MT, Perrin-Sarazin F, Cole KC, Denault J, Simard B (2005) Effect of carbon nanotubes on the crystallization and properties of polypropylene. J Polym Sci B 43:2445–2453
4. Assouline E, Lustiger A, Barber AH, Cooper CA, Klein E, Wachtel E, Wagner HD (2002) Nucleationability of multi wall carbon nanotubes in polypropylene composites. Polym Sci B 41: 520–527
5. Avouris PH, Hertel Y, Martel R, Schmidt T, Shea HR, Walkup RE (1999) Carbon nanotubes: nanomechanics, manipulation, and electronic devices. Appl Surf Sci 141:201–209
6. Treacy MMJ, Ebbesen TW, Gibson TM (1996) Exceptionally high Young's modulus observed for individual carbon nanotubes. Nature 381:678–680
7. Krishnan A, Dujardin E, Ebbesen TW, Yianilos PN, Treacy MM (1998) Young's modulus of single-walled nanotubes. Phys Rev B 58:14013–14019
8. Ashrafi B, Hubert P (2006) Modeling the elastic properties of carbon nanotube array/polymer composites. Compos Sci Technol 66:387–396
9. Paradise M, Goswami T (2007) Carbon nanotubes—production and industrial applications. Mater Des 28:1477–1489
10. Cheng SZD, Janimak JJ, Rodriguez J (1995) Crystalline structure of polypropylene homo- and copolymers. In: Polypropylene structure, blends and composites. Chapman and Hall, London
11. Lopez Manchado MA, Valentini L, Biagiotti J, Kenny JM (2005) Thermal and mechanical properties of single-walled carbon nanotubes–polypropylene composites prepared by melt processing. Carbon 43:1499–1505
12. Nobile MR, Simon GP, Valentino O, Marcom M (2007) Rheological and structure investigation of melt mixed multi-walled carbon nanotube/PE composites. Macromol Symp 247:78–87
13. Kwon JY, Kim HD (2005) Preparation and properties of acid-treated multiwalled carbon nanotube/waterborne polyurethane nanocomposites. J Appl Polym Sci 96:595–604
14. Bhattacharyya AR, Pötschke P (2006) Mechanical properties and morphology of melt-mixed PA6/SWNT composites: effect of reactive coupling. Macromol Symp 233:161–169
15. Feller JF, Linossier I, Pimbert S, Levesque G (2001) Carbon black-filled poly(ethelene-*co*-alkyl acrylate) composites: calorimetric studies. J Appl Polym Sci 79:779–793
16. Medeiros ES, Tocchetto RS, Carvalho LH, Santos LMG, Souza AG (2001) Nucleating effect and dynamic crystallization of a Poly(propylene)/talc system. J Therm Anal Calorim 66:523–531
17. Tjong SC, Bao SP, Liang GD (2005) polypropylene/montmorillonite nanocomposites toughened with SEBS-g-MA structure property relationship. J Polym Sci B 43:3112–3126
18. Qian JS, He PS, Nie KM (2004) Nonisothermal crystallization of PP/nano-$SiO_2$ composites. J Appl Polym Sci 91:1013–1019
19. Li GJ, Shi YY, Fan SR, Yu X (2007) Non-isothermal melt crystallization kinetics for poly(ethylene 2,6-naphthalate) (PEN)/montmorillonite nanocomposites prepared by melt intercalation. J Macromol Sci Phys 46:1231–1238
20. Wang L, Sheng J (2005) Nonisothermal crystallization kinetics of polypropylene/attapulgite nano-composites. J Macromol Sci Phys 44:31–42
21. Li Y, Wang S, Zhang Y, Zahng Y (2006) Crystallization behavior of carbon black-filled polypropylene and polypropylene/epoxy composites. J Appl Polym Sci 102:104–118
22. Yuan Q, Awate S, Misra RDK (2006) Nonisothermal crystallization behavior of polypropylene-clay nanocomposites. Eur Polym J 42:1994–2003
23. Jabarin SA (1987) Crystallization kinetics of polyethylene terephthalate. II Dynamic crystallization of PET. J Appl Polym Sci 34:97–102
24. Avrami M (1940) Kinetics of phase change. II Transformation-time relations for random distribution of nuclei. J Chem Phys 8:212–224
25. Lu XF, Hay JN (2001) Isothermal crystallization kinetics and melting behaviour of poly(ethylene terephthalate). Polymer 42:9423–9431

26. Hay JN, Sharma L (2000) Crystallization of (3-hydroxybutyrate)/polyvinyl acetate blends. Polymer 41:5749–5757
27. Zhou Z, Wang S, Lu L, Zhang Y, Zhang Y (2007) Isothermal crystallization kinetics of polypropylene with silane functionalized multi-walled carbon nanotubes. J Polym Sci B 45:1616–1624
28. Yuan Q, Awate S, Misra RDK (2006) Nonisothermal crystallization behavior of melt-intercalated polyethylene-clay nanocomposites. J Appl Polym Sci 102:3809–3818
29. Xue ML, Sheng J, Yu YL, Chuah HH (2004) Nonisothermal crystallization kinetics and spherulite morphology of poly(trimethylene terephthalate). Eur Polym J 40:811–818
30. Hay JN (1971) Application of the modified Avrami equations to polymer crystallisation kinetics. Br Polym J 3:74–82
31. Ozawa T (1971) Kinetics of non-isothermal crystallization. Polymer 12:150–156
32. Cazé C, Devaux E, Crespy A, Cavrot JP (1997) A new method to determine the Avrami exponent by DSC studies of nonisothermal crystallization from the molten state. Polymer 38:497–502
33. Chuah KP, Gan SN, Chee KK (1998) Polymer papers-determination of Avrami exponent by differential scanning calorimetry for non-isothermal crystallization of polymers. Polymer 40:253–259
34. An Y, Dong L, Mo Z, Liu T, Feng Z (1998) Nonisothermal crystallization kinetics of Poly($\beta$-hydroxybutyrate). J Polym Sci B 36:1305–1312
35. Liu T, Mo Z, Wang S, Zhang H (1997) Nonisothermal melt and cold crystallization kinetics of poly(aryl ether ether kethone kethone). Polym Eng Sci 37:568–575
36. Wang J, Dou Q (2007) Non-isothermal crystallization kinetics and morphology of isotactic polypropylene (iPP) nucleated with Rosin-based nucleating agents. J Macromol Sci Phys 46:987–1001
37. Ziabicki A (1971) Kinetics of polymer crystallization and molecular orientation in the course of fiber spinning. Appl Polym Symp 6:1–8
38. Ziabicki A (1974) Theoretical analysis of oriented and non-isothermal crystallization II. Extension of the Kolmogorotf-Avrami-Evans theory onto processes with variable rates and mechanisms. Colloid Polym Sci 252:433–435